# J|A|C|S

JOURNAL OF THE AMERICAN CHEMICAL SOCIETY

Article

Core/Shell Au/CuPt Nanoparticles and Their Dual Electrocatalysis for Both Reduction and Oxidation Reactions

Xiaolian Sun,[†] Dongguo Li,[†] Yong Ding,[‡] Wenlei Zhu,[†] Shaojun Guo,[†] Zhong Lin Wang,[‡] and Shouheng Sun*[,†]

[†]Department of Chemistry, Brown University, Providence, Rhode Island 02912, United States

[‡]School of Materials Science and Engineering, Georgia Institute of Technology, Atlanta, Georgia 30332, United States

ABSTRACT: We report a facile synthesis of monodisperse core/shell 5/1.5 nm Au/CuPt nanoparticles by coreduction of platinum acetylacetonate and copper acetylacetonate in the presence of 5 nm Au nanoparticles. The CuPt alloy effect and core/shell interactions make these Au/CuPt nanoparticles a promising catalyst for both oxygen reduction reactions and methanol oxidation reactions in 0.1 M $HClO_4$ solution. Their specific (mass) reduction and oxidation activities reach 2.72 mA/cm^2 (1500 mA/mg$_{Pt}$) at 0.9 V and 0.755 mA/cm^2 (441 mA/mg$_{Pt}$) at 0.8 V (vs reversible hydrogen electrode), respectively. Our studies show that the existence of the Au nanoparticle core not only minimizes the Pt usage but also improves the stability of the Au/CuPt catalyst for fuel cell reactions. The results suggest that the core/shell design is indeed effective for optimizing nanoparticle catalysis. The same concept may be extended to other multimetallic nanoparticle systems, making it possible to tune nanoparticle catalysis for many different chemical reactions.
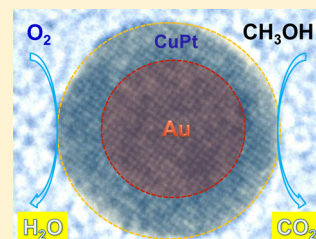
■ INTRODUCTION

Coupling fuel oxidation and oxygen reduction reactions at or near ambient conditions is an important approach to covert chemical energy stored in fuel to electric energy.[1] To ensure easy electron flow from fuel (via fuel oxidation) to oxygen (via oxygen reduction) at lower oxidation and reduction over-potentials, an efficient catalyst must be present to catalyze each of the two reactions.[2] Traditionally, nanoparticles (NPs) of Pt and its alloys with Ru are selected as such catalysts due to their relatively high activity and durability for both reactions in acidic media. Recently, the need to minimize the use of Pt has motivated the extended search for more efficient Pt NP catalysts with parameters tuned specifically for NP shapes,[3] Pt alloying with other early transition metals,[4] and core/shell structures.[5] Among these three classes of catalysts studied, shape and alloy composition-controlled catalysts often show some impressive enhancement in initial activity but have very limited improvement in stability unless the catalyst is prepared to have one-dimensional (1D) nanostructure.[6] Core/shell NPs, on the other hand, are found to be more promising as a robust catalyst. These Pt-based core/shell NPs with a non-Pt core not only maximize Pt exposure to reactants but also enhance Pt catalysis via strong core/shell interactions.[7] However, because of the difference in the chemical reaction nature between oxygen reduction and fuel oxidation reactions, these core/shell catalysts are often applied to a specific one. Therefore, different kinds of Pt catalysts have to be developed to improve the efficiency of these two reactions.

Herein we report a controlled synthesis of core/shell Au/CuPt NPs and demonstrate their enhanced dual catalysis for both oxygen reduction reaction (ORR) and methanol oxidation reaction (MOR) in 0.1 M $HClO_4$ solution. In studying core/shell NPs as a robust catalyst for fuel cell reactions, we noticed that Au/FePt$_3$ NPs with a 1.5 nm FePt$_3$ shell showed much improved activity and durability in catalyzing ORR in 0.1 M $HClO_4$ solution[5a] while FePt/PtAu with FePt in face-centered tetragonal structure and Au segregating around the Pt shell were highly efficient for formic acid oxidation reaction (FAOR) and MOR.[8] However, they became ineffective if their role was switched. Interestingly, core/shell CuPt/Pt NPs made from controlled dealloying of Cu from CuPt NPs showed enhanced ORR catalysis,[7a] and cubic CuPt NPs were found to be active for FAOR and MOR with enhanced CO tolerance.[9] This indicated that CuPt as a catalyst component was capable of serving as a catalyst for both ORR and fuel oxidation reactions. Therefore, we synthesized core/shell Au/CuPt NPs via a seed-mediated growth method and expected that the CuPt shell would exhibit dual catalysis and the Au core would further enhance the catalysis by stabilizing the CuPt shell. Our tests showed that these Au/CuPt NPs were indeed efficient in its dual catalysis for both ORR and MOR. Its ORR and MOR specific (mass) activities reached 2.72 mA/cm^2 (1500 mA/mg$_{Pt}$) at 0.9 V and 0.755 mA/cm^2 (441 mA/mg$_{Pt}$) at 0.8 V (vs reversible hydrogen electrode, RHE), respectively.

■ EXPERIMENTAL SECTION

Materials. 1-Octadecene (ODE), borane *tert*-butylamine complex (BBA), oleic acid (OA), 1,2,3,4-tetrahydronaphthalene (tetralin), platinum acetylacetonate (Pt(acac)$_2$), copper acetylacetonate (Cu-(acac)$_2$), 1,2-hexadecanediol (HDD), Nafion 117, and carbon black (Ketjen EC 300J) were all from Sigma Aldrich. Oleylamine (OAm) was from Acros Organics. HAuCl$_4$·3H$_2$O was from Strem Chemicals. All chemicals were used as received.

Instruments. Transmission electron microscopy (TEM) images were acquired on a Philips EM 420 (120 kV). High resolution TEM (HRTEM) images were obtained on a JEOL 2010 TEM (200 kV). High resolution high angle annular dark-field scanning TEM (HAADF-STEM) and elemental mapping images were obtained on a JEOL 2200FS microscope with a beam size of ~0.8 Å for imaging and ~2 Å for chemical analysis. All TEM samples were prepared by depositing a drop of diluted NP dispersion in hexane on a copper grid coated with amorphous carbon. X-ray diffraction (XRD) patterns were collected on a Bruker AXS D8-Advanced diffractometer with Cu Kα radiation (λ = 1.5418 Å). The inductively coupled plasma mass spectrometry (ICP-AES) analyses were performed on a JY2000 Ultrace ICP atomic emission spectrometer equipped with a JY AS 421 autosampler and 2400 g/mm holographic grating. Energy dispersive X-ray spectroscopy (EDS) was carried out on a JEOL JSM-6060 scanning electron microscope (SEM). Samples for EDS were deposited on a graphitized porous carbon support. UV−vis spectra were recorded on a Perkin-Elmer Lambda 35 spectrometer. Electrochemical measurements were carried out on a Pine electrochemical analyzer, model AFCBP1. Ag/AgCl (filled with 0.1 M KNO$_3$) and Pt wire were used as reference and counter electrodes, respectively. All potentials were calibrated against reversible hydrogen electrode (RHE).

Synthesis of Au NPs. Au NPs were synthesized through adopting the previous protocol.[10] HAuCl$_4$·3H$_2$O (0.2 g) was dissolved in tetralin (10 mL) and OAm (10 mL), and the solution was cooled in an ice bath (0 °C). BBA (1 mmol), tetralin (1 mL), and OAm (1 mL) were mixed by sonication and quickly injected into the above solution. The reaction mixture was further stirred at room temperature for 3 h. Au NPs were precipitated by adding acetone and collected by centrifugation. The product was redispersed in hexane and separated by adding ethanol and centrifugation. The final product was dispersed in hexane.

Synthesis of Au/CuPt Core/Shell NPs. Cu(acac)$_2$ (0.25 mmol) Pt(acac)$_2$ (0.25 mmol) and HDD (2 mmol) were dissolved in 10 mL of ODE before Au NPs (35 mg) in hexane (1 mL) were added. The mixture was heated to 120 °C under a gentle N$_2$ flow to remove hexane before it was heated to 200 °C at a heating rate of 2 °C/min and kept at this temperature for 30 min. The reaction mixture was cooled to room temperature. The product was precipitated by 2-propanol and collected by centrifugation. The product was redispersed in hexane and separated by adding ethanol and centrifugation. The final product was dispersed in hexane.

Electrochemical Measurements. Ten milligrams of the as-synthesized NPs and 20 mg of Ketjen-300J carbon support were mixed in 10 mL of hexane and sonicated with a Fischer Scientific FS 110 for 60 min. The product was then suspended in 20 mL of acetic acid at 60 °C overnight under a mild N$_2$ flow. The catalyst (C-NPs) was separated by centrifugation and washed with ethanol three times before it was suspended in deionized water at a concentration of 2 mg/mL. Nafion (0.5% v/v) was added, and the suspension was sonicated for 1 h.

Ten microliters of C-NPs in water was dropped on a rotation disk electrode (RDE) with a glassy carbon surface (5 nm in diameter from Hokuto Denko Corp., Japan). Water was slowly evaporated in the air, and another 10 μL of C-NPs was dropped on the electrode and dried to ensure a complete coverage of electrode surface.

Surface cleaning was carried out by CV scanning in N$_2$ saturated 0.1 M HClO$_4$ at room temperature between 0.05 and 1.20 V at a scan rate of 50 mV/s for 100 scans. CO stripping voltammetry was performed by scanning between 0.05 and 1.10 V in Ar-purged 0.1 M HClO$_4$ at 50 mV/s after a CO$_{adlayer}$ was formed on the NP surface in the CO-saturated 0.1 M HClO$_4$ at 0.10 V. Oxygen reduction reaction (ORR) catalyzed by C-NPs was measured by a rotation disk electrode at 1600 rpm and 20 mV/s. The catalyst stability was checked by scanning between 0.60 and 1.10 V at 100 mV/s for 5000 sweeps. Methanol oxidation reaction (MOR) catalyzed by the same C-NPs was evaluated in N$_2$-saturated 0.1 M HClO$_4$ containing 0.1 M methanol at room temperature. The CV scan was carried out between 0.3 and 1.2 V with

a scan rate of 20 mV/s. The stability was tested by chronoamperometry at 0.8 V for 1 h.

■ RESULTS AND DISCUSSION

The core/shell Au/CuPt NPs were prepared by simultaneous reduction of Pt(acac)$_2$ and Cu(acac)$_2$ in the mixture of 5 nm seeding Au NPs, HDD, OAm, OA, and ODE at 200 °C. In the synthesis, Au NPs were premade and coated with OAm. HDD served as a reducing agent and OA/OAm as surfactants. This seed-mediated growth condition facilitated CuPt deposition around each Au NP, forming core/shell Au/CuPt with a uniform shell of CuPt. CuPt compositions were controlled by the molar ratio of Cu(acac)$_2$ to Pt(acac)$_2$ and analyzed by ICP-MS and EDS. For example, Pt$_{65}$Cu$_{35}$, Pt$_{50}$Cu$_{50}$, and Pt$_{36}$Cu$_{64}$ were obtained from 3:2, 1:1, and 3:5 Pt/Cu ratios, respectively.

Figure 1a,b shows the typical TEM images of the seeding 5 nm Au NPs and the core/shell NPs. After CuPt coating, the
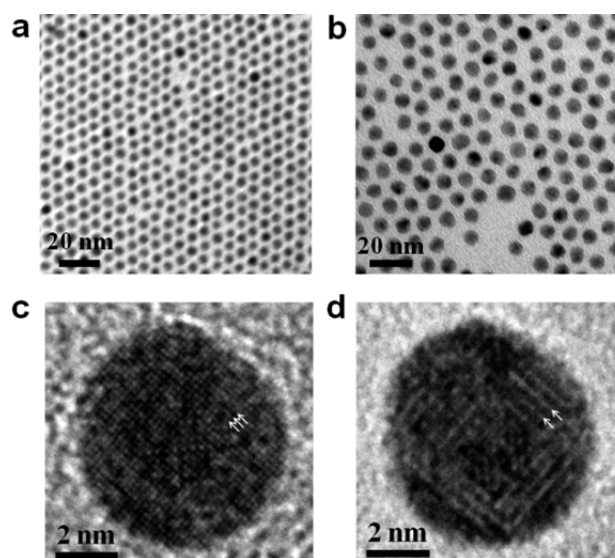

Figure 1. TEM images of (a) 5 nm Au NPs, (b) 7.5 nm Au/Cu$_{35}$Pt$_{65}$ NPs. (c, d) HRTEM images of a single Au/Cu$_{35}$Pt$_{65}$ NP acquired at a different focus condition.

average size of the core/shell NPs was increased from 5 ± 0.5 nm (Au NPs) to 7.5 ± 0.5 nm (Au/CuPt), indicating the coating thickness was at 1.3 nm. High resolution TEM (HRTEM) was used to analyze the detailed structure of a single NP, as shown in Figure 1c,d. The interface between the Au core and Pt shell cannot be clearly seen because of the close scattering power and lattice paramter of Au and Pt in the core and shell structure. There is also no clear evidence of the existence of misfit dislocation, as observed in the Au/FePt system.[11] However, the HRTEM image of the same NP (Figure 1c) recorded at different focus conditions (Figure 1d) shows a long-range ordered structure as highlighted by the arrowheads, which must come from the CuPt alloy structure. The formation of the ordered structure indicates that CuPt is successfully coated over the Au core. The core/shell structure was further confirmed by the linear EDS scan across a single particle (Figure 2). Operated at 300 kV, EDS revealed that the Au peak was 1 nm narrower than the Pt peak at the beginning of the scan (the left side of the line scan, Figure 2a,b), indicating that the coating thickness was around 1 nm. However, at the end of the scan, the NP showed an alloy-type structure (Figure 2b). We also obtained the image of the NP we scanned and noticed
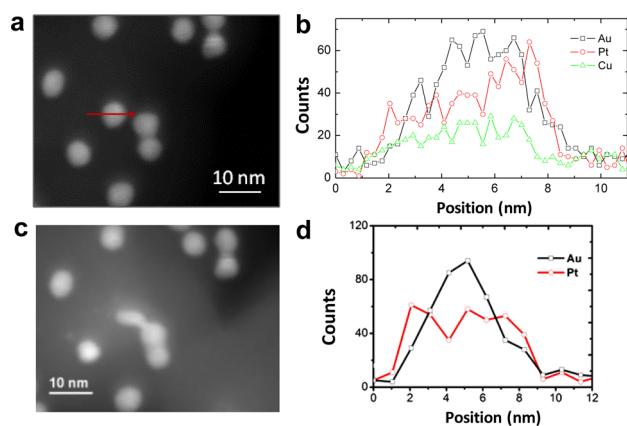
Figure 2. (a) HAADF-STEM image of the Au/CuPt NPs before the EDS scan at 300 kV, (b) line-scan EDS analysis across a single Au/CuPt NP indicated in panel a, (c) HAADF-STEM image of the same Au/CuPt NPs shown in panel a after the EDS scan at 300 kV, indicating the diffusion between the core and shell, and (d) line-scan EDS analysis across a single Au/CuPt NP at 200 kV.

the morphology change upon electron beam irradiation (Figure 2c). However, when the operation voltage was decreased to 200 kV, the EDS analysis showed clearly the core/shell structure (Figure 2d). This indicates that the core/shell Au/CuPt is indeed formed and that the high voltage electron beam used for EDS analysis can trigger the core/shell diffusion into the solid solution structure.

In the synthesis, the ratio of Au seeds over $Pt(acac)_2$ was kept the same and the amount of $Cu(acac)_2$ was used to control Cu/Pt compositions. Figure 3a is the plot of atomic % of Cu in
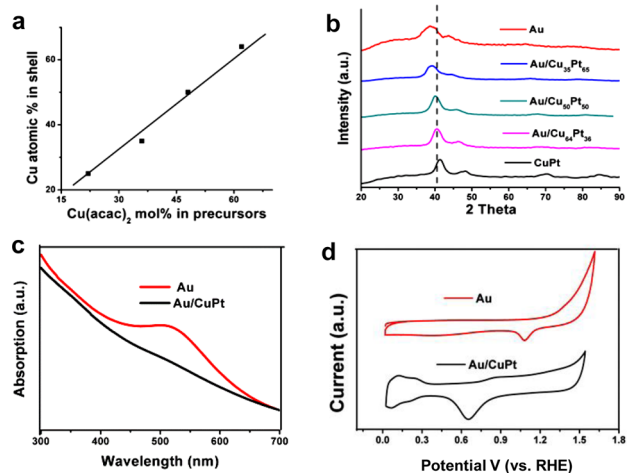

Figure 3. (a) Correlation between the amount of $Cu(acac)_2$ added and the amount of Cu obtained in the final CuPt shell (b) XRD pattern of Au/Cu_xPt_{1-x} (x = 35, 50, 64) core/shell NPs. (c) UV–vis spectra of the 5 nm Au NPs and Au/CuPt NPs in hexane. (d) CVs of the C-Au and C-Au/CuPt in N_2-saturated 0.1 M $HClO_4$ solution.

the CuPt shell vs mol % $Cu(acac)_2$ used to react with 0.25 mmol of $Pt(acac)_2$ in coating CuPt over Au NPs. The molar percentage of Cu in the shell structure (y-axis) is nearly the same as that of $Cu(acac)_2$ in the two precursors ($Cu(acac)_2$ and $Pt(acac)_2$) (x-axis), which indicates that the Cu/Pt compositions are carried over to the final CuPt shell under our synthetic conditions. Figure 3b shows the XRD patterns of the Au/Cu_xPt_{1-x} (x = 35, 50, 64) core/shell NPs and pure CuPt NPs.

The (111) diffraction of the Au NPs appears at 38° while that of the $Cu_{50}Pt_{50}$ NPs at 41.4°. Once the CuPt shell is coated on Au, the CuPt (111) peak appears between Au (111) and CuPt (111) peaks, indicating that the (111) lattice in the CuPt shell is increased compared to that in pure CuPt NPs due to the Au core effect. With more Cu present in the CuPt structure, the (111) peak shifts from 39.5° (Au/$Cu_{35}Pt_{65}$), to 40.2° (Au/$Cu_{50}Pt_{50}$), to 40.8° (Au/$Cu_{64}Pt_{36}$), which follows Vegard's Law[12] and proves the formation of CuPt alloy structure. Incorporating more Cu in the CuPt shell led to a slight increase in shell thickness. For example, Au/$Cu_{35}Pt_{65}$ has a 1 nm shell, and Au/$Cu_{64}Pt_{36}$ has a 1.5 nm shell. The CuPt coating was further characterized by UV–vis spectroscopy and electrochemical redox properties. The surface plasmonic absorption peak of the 5 nm Au NPs in hexane dispersion appeared at 520 nm. UV–vis spectra of the core/shell NP dispersion in hexane showed no plasmonic absorption (Figure 3c). To test the electrochemical properties of these NPs, we first deposited the NPs on the Ketjen carbon support by sonicating for 1 h a mixture of NPs and carbon support in 5 mL of hexane at a weight ratio of 1:2. We then used acetic acid and 0.1 M $HClO_4$ solution to wash the C-NP composite to remove the surfactants around each NP.[13] These combined acid treatments did not change either Au/Pt ratio or Cu composition. Cyclic voltammgrams (CVs) of the NPs recorded from 0.02 to 1.61 V in N_2-saturated 0.1 M $HClO_4$ is given in Figure 3d. We can see that the C-Au NPs have a Au-O-related reduction peak at 1.08 V, while C-Au/CuPt NPs show only CuPt-O and no Au-O reduction peak, indicating that Au is embedded under the CuPt shell.

Cu in the Au/CuPt NPs could be further etched away electrochemically, forming Au/CuPt/Pt core/shell NPs. This was similar to the electrochemical dealloying of Cu observed in CuPt NPs.[7a,14] Figure 4a lists several rounds of CV scans for

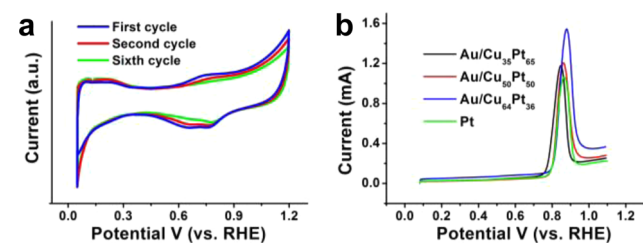**Figure 4.** (a) CV curves of the C-Au/$Cu_{64}Pt_{36}$ catalyst during electrochemical dealloying at 100 mV/s. (b) CO stripping curves of the C-Au/Cu_xPt_{100-x} and C-Pt catalysts in 0.1 M $HClO_4$.

the Au/$Cu_{64}Pt_{36}$ NPs. In the first anodic scan, there is a broad peak near 0.6−0.7 V which refers to the Cu dissolving process from the CuPt shell. In the backward cathodic scan, there are two peaks related to the reduction of Pt-O (0.8 V) and Cu-O oxide (0.6 V). During the second scan, the area of the Cu dissolving peak decreased dramatically and the hydrogen desorption peak (0.04−0.4 V) increased, indicating the removal of surface Cu and the formation of the Pt layer. Once the dealloying reached equilibrium and there was no hydrogen desorption peak increase (after 50 cycles), Au/$Cu_{50}Pt_{50}$ and Au/$Cu_{64}Pt_{36}$ were converted to Au/$Cu_{36}Pt_{64}$, and Au/$Cu_{35}Pt_{65}$ was converted to Au/$Cu_{29}Pt_{71}$. The CO stripping peak of the dealloyed Au/$Cu_{36}Pt_{64}$ (Figure 4b) resembled that of the pure Pt[5a] and core/shell FePtCu/Pt nanorods,[15] confirming that Au/$Cu_{36}Pt_{64}$ NPs have a smooth Pt shell, forming Au/CuPt/Pt.

The electrocatalytic activity of these Au/CuPt (Au/CuPt/Pt) NPs for the ORR was studied. Figure 5a shows the
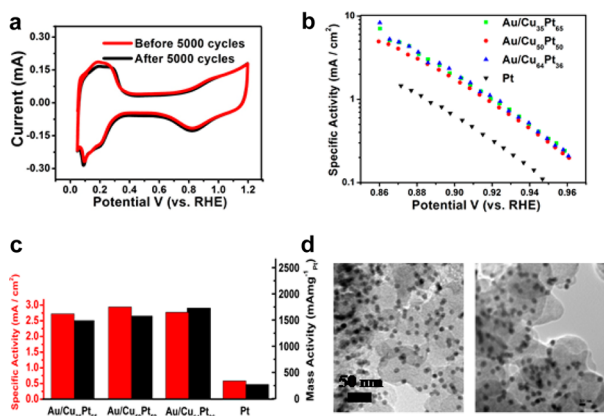

Figure 5. (a) CVs of C-Au/Cu₃₅Pt₆₅ NPs before and after 5000 potential cycles between 0.6 and 1.0 V. (b) Activity−potential plots of C-Au/Cu$_x$Pt$_{100-x}$ and C-Pt catalysts. (c) Specific and Pt mass activities of C-Au/Cu$_x$Pt$_{100-x}$ and C-Pt catalysts at 0.9 V. (d) TEM of C-Au/Cu₃₅Pt₆₅ NPs before (left) and after (right) 5000 potential cycles.

representative CV curves obtained in N_2-saturated 0.1 M $HClO_4$ solution. The ORR polarization curves were obtained in O_2-saturated 0.1 M $HClO_4$ solution. The Tafel plots of three C-NPs (Au/Cu₃₅Pt₆₅, Au/Cu₅₀Pt₅₀, and Au/Cu₆₄Pt₃₆) are given in Figure 5b. By comparing CV and ORR curves of different Au/CuPt NPs, we noticed that the specific activities of the core/shell NPs were not Cu composition dependent. This is likely caused by the dealloying of Cu (leaving only 25−36% Cu present in the final core/shell structure) and the formation of the Pt shell. The specific activities of the Au/CuPt reach as high as 2.75 mA/cm^2 at 0.9 V which is nearly five times higher than that from the 5 nm commercial Pt (commercial TKK TEC10E50E-HT 5 nm Pt 50.5% wt Pt loading) (0.58 mA/cm^2). Figure 5c lists the specific and mass activities of the core/shell NPs and Pt NPs for ORR. The core/shell NPs have mass activity up to 1700 mA/mg$_{Pt}$ at 0.9 V (from the Au/Cu₆₄Pt₃₆ NPs), six times higher than that of the commercial 5 nm Pt (270 mA/mg$_{Pt}$). The stability of the Au/CuPt NPs was also tested by performing 5000 potential sweeps between 0.60 and 1.10 V at 100 mV/s in O_2-saturated 0.1 M $HClO_4$ solution. Figure 5a shows the CV s of the Au/Cu₃₅Pt₆₅ NPs before and after the test. The ECASA of the Au/CuPt dropped only 7.8% after this stability test while that of the commercial Pt decreased by 20%. TEM analysis further confirmed the stability of the Au/CuPt NPs, as they showed little morphology change after the stability test (Figure 5d).

The Au/CuPt NPs were also an active catalyst for MOR. Figure 6 summarizes the CV oxidation and stability test results. Among all core/shell NPs studied, the Au/Cu₆₄Pt₃₆ NPs showed the highest catalytic activity (Figure 6a). Even after a 1 h stability test, the catalytic activity of the Au/Cu₆₄Pt₃₆ NPs was still much higher than that of Pt (Figure 6b). This high activity is attributed to the high CO tolerance of the Au/CuPt NPs as characterized by the current ratio change between two peaks in forward (I_f) and backward (I_b) scans in the CV; the larger the ratio, the better the CO removal activity of the catalyst.[16] The mass activity of the Au/Cu₆₄Pt₃₆ NPs was calculated to be around 441 mA/mg$_{Pt}$, four times higher than that of Pt NPs at 0.8 V.
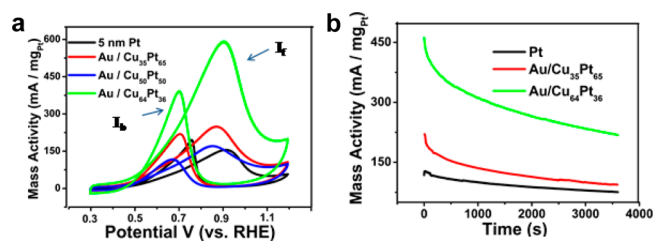

Figure 6. (a) MOR curves and (b) catalyst stability test at 0.8 V in 0.1 M $HClO_4$ + 0.1 M methanol.

The observed enhancement of the Au/CuPt NPs on both ORR and MOR catalysis is likely caused by the combination of alloy and strain effects present in the core/shell structure. Similar to what has been predicted and observed, alloying Pt with an early transition metal lowers the Pt d-band level, weakening the binding of oxygenated spectator (blocking) species (e.g., OH$^-$) to Pt and increasing the number of active Pt sites that are accessible to oxygen.[17] The formation of Au/CuPt/Pt may also have the surface Pt lattice compressed, further favoring ORR.[7a] The presence of electropositive Au in the core can prevent Pt from being easily oxidized,[5a,18] stabilizing the Pt shell in the ORR condition. The Au core and Cu alloying effects must also help methanol adsorption/activation on Pt with high CO tolerance, rendering the Au/CuPt/Pt NPs equally effective in catalyzing MOR.

In conclusion, we have reported a facile synthesis of monodisperse 5/1.5 nm Au/CuPt NPs by coreduction of Pt(acac)₂ and Cu(acac)₂ in a mixture of 5 nm seeding Au NPs, HDD, OAm, OA, and ODE at 200 °C. The Au core provides the proper nucleation sites for CuPt alloy formation, and as a result, the nucleation/growth of the CuPt shell occurs at a lower temperature without the formation of free CuPt NPs. Due to the CuPt alloy effect and core/shell interactions, these Au/CuPt NPs show promising dual catalysis for both ORR and MOR in 0.1 M $HClO_4$ solution with their ORR specific (mass) activities reaching 2.72 mA/cm^2 (1500 mA/mg$_{Pt}$) at 0.9 V and MOR specific (mass) activities at 0.755 mA/cm^2 (441 mA/mg$_{Pt}$) at 0.8 V. Our tests prove that the existence of the Au NP core not only minimizes the Pt usage in its catalysis for fuel cell reactions but also improves drastically the stability of the core/shell catalyst. The results suggest that the core/shell design is indeed effective for optimizing NP catalysis. The same concept may be extended to other multimetallic NP system, making it possible to tune NP catalysis for many different chemical reactions.

■ AUTHOR INFORMATION

Corresponding Author
ssun@brown.edu

Notes

The authors declare no competing financial interest.

■ ACKNOWLEDGMENTS

D

dx.doi.org/10.1021/ja500590n | *J. Am. Chem. Soc.* XXXX, XXX, XXX−XXX

■ REFERENCES

(1) (a) Reed, T. B.; Lerner, R. M. *Science* **1973**, *182*, 1299−1304. (b) Barbir, F. *PEM Fuel Cells: Theory and Practice*; Academic Press: New York, 2005; pp 1−38.

(2) (a) Mark, K. D. *Nature* **2012**, *486*, 43−51. (b) Zhang, J. *PEM Fuel Cell Electrocatalysts and Catalyst Layers: Fundamentals and Applications*; Springer: New York, 2008; pp 355−373. (c) Wieckowski, A. *Fuel Cell Catalysis: A Surface Science Approach*; Wiley-VCH: Weinheim, 2008; pp 271−375.

(3) (a) Wang, C.; Daimon, H.; Onodera, T.; Koda, T.; Sun, S. *Angew. Chem., Int. Ed.* **2008**, *47*, 3588−3591. (b) Porter, N. S.; Wu, H.; Quan, Z.; Fang, J. *Acc. Chem. Res.* **2013**, *46*, 1867−1877. (c) Kang, Y.; Li, M.; Cai, Y.; Cargnello, M.; Diaz, R. E.; Gordon, T. R.; Wieder, N. L.; Adzic, R. R.; Gorte, R. J.; Stach, E. A.; Murray, C. B. *J. Am. Chem. Soc.* **2013**, *135*, 2741−2747.

(4) (a) Wang, C.; Markovic, N. M.; Stamenkovic, V. R. *ACS Catal* **2012**, *2*, 891−898. (b) Zhang, J.; Fang, J. *J. Am. Chem. Soc.* **2009**, *131*, 18543−18547. (c) Wu, J.; Qi, L.; You, H.; Gross, A.; Li, J.; Yang, H. *J. Am. Chem. Soc.* **2012**, *134*, 11880−11883.

(5) (a) Wang, C.; Vliet, D.; More, K. L.; Zaluzec, N. J.; Peng, S.; Sun, S.; Daion, H.; Wang, G.; Greeley, J.; Pearson, J.; Paulikas, A. P.; Karapetrov, G.; Strmcnik, D.; Markovic, N. M.; Stamenkovic, V. R. *Nano Lett.* **2011**, *11*, 919−926. (b) Mazumder, V.; Chi, M.; More, K. L.; Sun, S. *J. Am. Chem. Soc.* **2010**, *132*, 7848−7849. (c) Gong, K.; Su, D.; Adzic, R. R. *J. Am. Chem. Soc.* **2010**, *132*, 14364−14366. (d) Koenigsmann, C.; Santulli, A. C.; Gong, K.; Vukmirovic, M. B.; Zhou, W.; Sutter, E.; Wong, S. S.; Adzic, R. R. *J. Am. Chem. Soc.* **2011**, *133*, 9783−9795.

(6) Guo, S.; Li, D.; Zhu, H.; Zhang, S.; Markovic, N. M.; Stamenkovic, V. R.; Sun, S. *Angew. Chem., Int. Ed.* **2013**, *52*, 3465−3468.

(7) (a) Strasser, P.; Koh, S.; Anniyev, T.; Greeley, J.; More, K; Yu, C.; Liu, Z.; Kaya, S.; Nordlund, D.; Ogasawara, H.; Toney, M. F.; Nilsson, A. *Nat. Chem.* **2010**, *2*, 454−460. (b) Hwang, S.; Yoo, S.; Shin, J.; Cho, Y.; Jang, J.; Cho, E.; Sung, Y.; Nam, S.; Lim, T.; Lee, S.; Kim, S. *Sci. Rep.* **2012**, *3*, 1309.

(8) Zhang, S.; Guo, S.; Zhu, H.; Su, D.; Sun, S. *J. Am. Chem. Soc.* **2012**, *134*, 5060−5063.

(9) (a) Xu, D.; Liu, Z.; Yang, H.; Liu, Q.; Zhang, J.; Fang, J.; Zhou, S.; Sun, S. *Angew. Chem., Int. Ed.* **2009**, *48*, 4217−4221. (b) Xu, D.; Bliznakov, S.; Liu, Z.; Fang, J.; Dimitrov, N. *Angew. Chem.* **2010**, *122*, 1304−1307.

(10) Peng, S.; Lee, Y.; Wang, C.; Yin, H.; Dai, S.; Sun, S. *Nano Res.* **2008**, *1*, 229−234.

(11) Ding, Y.; Sun, X.; Wang, Z. L.; Sun, S. *Appl. Phys. Lett.* **2012**, *100*, 111603.

(12) Denton, A. R.; Ashcroft, N. W. *Phys. Rev. A* **1991**, *43*, 3161−3164.

(13) Mazumder, V.; Sun, S. *J. Am. Chem. Soc.* **2009**, *131*, 4588−4589.

(14) (a) Koh, S.; Strasser, P. *J. Am. Chem. Soc.* **2007**, *129*, 12624−12625. (b) Gupta, G.; Slanac, D. A.; Kumar, P.; Wiggins-Camacho, J. D.; Wang, X.; Swinnea, S.; More, K. L.; Dai, S.; Stevenson, K. J.; Johnston, K. P. *Chem. Mater.* **2009**, *21*, 4515−4526.

(15) Zhu, H.; Zhang, S.; Guo, S.; Su, D.; Sun, S. *J. Am. Chem. Soc.* **2013**, *135*, 7130−7133.

(16) Sharma, S.; Ganguly, A.; Papakonstantinou, P.; Miao, X.; Li, M.; Hutchison, J. L.; Delichatsios, M.; Ukleja, S. *J. Phys. Chem. C* **2010**, *114*, 19459−19466.

(17) (a) Stamenkovic, V. R.; Fowler, B.; Mun, B. S.; Wang, G. F.; Ross, P. N.; Lucas, C. A.; Markovic, N. M. *Science* **2007**, *315*, 493−497. (b) Wang, C.; Markovic, N. M.; Stamenkovic, V. R. *ACS Catal.* **2012**, *2*, 891−898. (c) Greeley, J.; Stephens, I. E. L.; Bondarenko, A. S.; Johansson, T. P.; Hansen, H. A.; Jaramillo, T. F.; Rossmeisll, J.; Chorkendorff, I.; Nørskov, J. K. *Nat. Chem.* **2009**, *1*, 552−556.

(18) Zhang, J.; Sasaki, K.; Sutter, E.; Adzic, R. R. *Science* **2007**, *315*, 220−222.